Initial Results from the EUV Engineering Test Stand

Daniel A. Tichenor[*a], Avijit K. Ray-Chaudhuri[b], Sang H. Lee[f], Henry N. Chapman[d], William C. Replogle[a], Kurt W. Berger[a], Richard H. Stulen[a], Glenn D. Kubiak[a], Leonard E. Klebanoff[a], John B. Wronosky[c], Donna J. O'Connell[a], Alvin H. Leung[a], Karen L. Jefferson[a], William P. Ballard[a], Layton C. Hale[d], Kenneth Blaedel[d], John S. Taylor[d], James A. Folta[d], Eberhard Spiller[d], Regina Soufli[d], Gary E. Sommargren[d], Donald W. Sweeney[d], Patrick Naulleau[e], Kenneth A. Goldberg[e], Eric M. Gullikson[e], Jeffrey Bokor[e], David T. Attwood[e], Uwe Mickan[g], Ralph Hanzen[g], Eric Panning[f], Pei-Yang Yan[f], John E. Bjorkholm[f], and Charles W. Gwyn[f]

[a]Sandia National Laboratories, PO Box 969, Livermore CA 94551
[b]formerly with Sandia National Laboratories, PO Box 969, Livermore CA 94551
[c]Sandia National Laboratories, PO Box 5800, Albuquerque NM 87185
[d]Lawrence Livermore National Laboratory, PO Box 808, Livermore, CA 94550
[e]Lawrence Berkeley National Laboratory, One Cyclotron Road, Berkeley, CA 94720
[f]Intel Corporation, 2200 Mission College Boulevard, Santa Clara CA 95052
[g]ASML Veldhoven, The Netherlands

ABSTRACT

The Engineering Test Stand (ETS) is an EUV lithography tool designed to demonstrate full-field EUV imaging and provide data required to accelerate production-tool development. Early lithographic results and progress on continuing functional upgrades are presented and discussed. In the ETS a source of 13.4 nm radiation is provided by a laser plasma source in which a Nd:YAG laser beam is focused onto a xenon-cluster target. A condenser system, comprised of multilayer-coated and grazing incidence mirrors, collects the EUV radiation and directs it onto a reflecting reticle. The resulting EUV illumination at the reticle and pupil has been measured and meets requirements for acquisition of first images.

Tool setup experiments have been completed using a developmental projection system with ?/14 wavefront error (WFE), while the assembly and alignment of the final projection system with ?/24 WFE progresses in parallel. These experiments included identification of best focus at the central field point and characterization of imaging performance in static imaging mode. A small amount of astigmatism was observed and corrected in situ, as is routinely done in advanced optical lithographic tools. Pitch and roll corrections were made to achieve focus throughout the arc-shaped field of view. Scan parameters were identified by printing dense features with varying amounts of magnification and skew correction. Through-focus scanned imaging results, showing 100 nm isolated and dense features, will be presented. Phase 2 implementation goals for the ETS will also be discussed.

Keywords: EUVL, lithography, laser-produced plasma, laser plasma source

1. INTRODUCTION

Extreme Ultraviolet Lithography (EUVL) is widely regarded as the leading candidate for printing dense features down to 30 nm with introduction as early as the 70 nm node. To support the commercialization of EUVL, an alpha -class tool, called the EUV Engineering Test Stand (ETS), has been developed. Full-field printing of high resolution EUV images has been demonstrated in both static and step-and-scan mode. Ongoing work with the ETS is providing the system learning required to develop commercial EUVL tools[1]. EUVL technology development is funded by the EUV Limited Liability Company (LLC), a consortium of semiconductor manufacturers founded in 1997 and comprised of Advanced Micro Devices, Infineon, Intel, IBM, Micron, and Motorola. The Department of Energy Virtual National Laboratory, comprised of Lawrence Berkeley National Laboratory, Lawrence Livermore National Laboratory and Sandia National Laboratories, perform research, development, and engineering to accelerate the commercialization of EUVL.

To meet the EUVL learning objective, the lithographic performance of the ETS is being characterized in its initial configuration in which a developmental projection system, PO Box 1, is installed. The initial configuration also utilizes a

* Correspondence: Email: datiche@sandia.gov; Telephone: 925 294 2137; Fax: 925 294 3870

low power (40 watt) drive laser for the laser-produced plasma source. Baseline results subject to these limitations have been acquired for comparison to the ETS performance as system improvements continue to be implemented.

A number of significant results have been acquired to date. First, a small amount of astigmatism has been identified in PO Box 1 by using printed resist images. Analytical quantification and in situ correction of this aberration has been demonstrated. The ETS 6-channel pupil-illumination fill profile has been measured, and the effects on the imaging characteristics have been modeled. Condenser designs for commercial tools will provide a conventional fill profile and eliminate this effect. The demonstrated ETS field size of 24 mm by 32.5 mm is the largest high-resolution EUV field printed to date. Skew and scan magnification parameters have been determined experimentally. Using these parameters scanned images of comparable quality to ETS static images have been printed. Initial flare measurements have been acquired near the central field point and compared to modeling results. ETS characterization is aided by the implementation of a variety of sensor systems including the recent demonstration of an Aerial Image Monitor, AIM, that measures image characteristics in situ in near real time.

Major ETS system upgrades are in progress. The first upgrade increases the drive laser power to 1500 watts and incorporates thermal and target-system improvements required to sustain operation at this power level. The second upgrade replaces PO Box 1 with an improved projection system, PO Box 2, having lower figure error and lower flare. Small-field static images, acquired using PO Box 2, demonstrate that the desired improvements in image performance have been realized in the central field region. To support these enhanced capabilities, the stage system is being modified to improve reliability and achieve faster scanning with low jitter.

2. ETS DESIGN OVERVIEW

The ETS design incorporates two vacuum enclosures that provide for independent control of the vacuum environment. The source module houses the laser-produced plasma (LPP) source and illumination system, and the main module houses the projection optics and stage system (See Fig. 1). A pulsed Nd:YAG laser beam is introduced through a window in the source enclosure and is incident on a xenon-jet target to produce EUV radiation. A system of vacuum pumps extracts the resulting xenon gas from the enclosure and delivers it to a xenon re-circulation system. A six-channel condenser collects radiation from the source and directs it into the main chamber, where a final condenser element shapes the beam to illuminate the arc-shaped field of view of the projection system. A spectral-purity filter, comprised of a Zr foil supported by a Ni wire mesh, removes out-of-band radiation and provides an environmental barrier between the source and main enclosures.

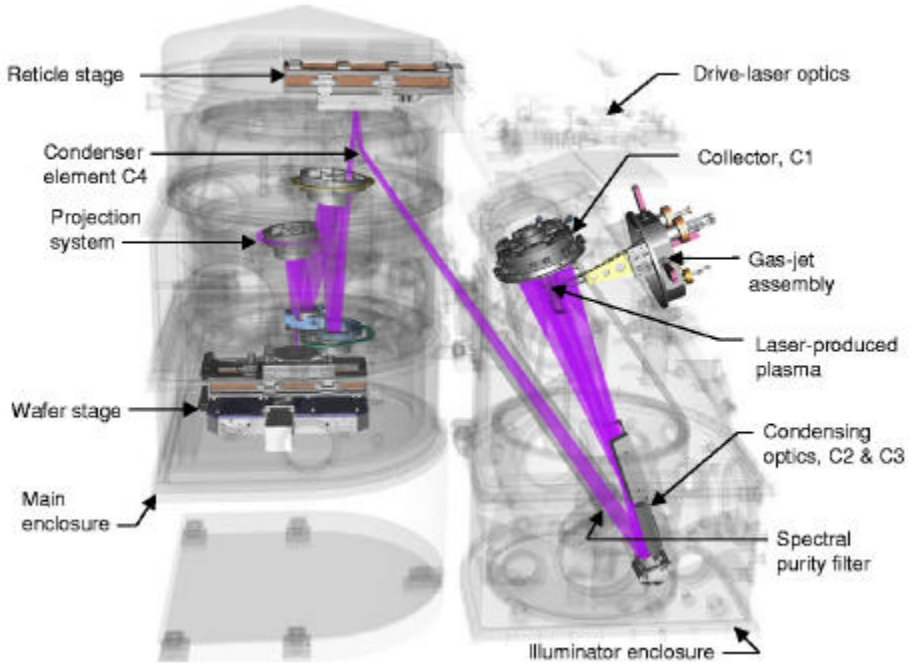

Figure 1. Solid model of the EUV Engineering Test Stand.

In the main enclosure radiation from the final condensing element illuminates an arc-shaped field on a reflecting reticle. The reticle is carried on a magnetically levitated stage that provides one long dimension of travel for scanning and five short-travel degrees of freedom for reticle alignment. EUV radiation reflected from the reticle is imaged using a 4 mirror, 4x reduction projection system having a numerical aperture of 0.1 at the wafer. A resist-coated wafer is clamped using an electrostatic chuck and carried on a second 1-D long-travel magnetically levitated stage, which is carried on mechanical stage to achieve full wafer coverage in the non-scan direction. The ETS is extensively instrumented with pressure, temperature, vibration and flux sensors to achieve the data gathering objective. Where additional diagnostics are needed, the ETS incorporates special sensors, including a system for viewing the fill profile at the projection system aperture, a through-the-lens-visible imaging system and an Aerial Image Monitor, AIM, for in situ measurement of the EUV aerial image.

3. INITIAL LITHOGRAPHIC RESULTS

Characterization of the ETS using PO Box 1 and a low power drive laser is intended to provide a baseline performance metric to which future results can be compared as the major system upgrades are implemented. Several areas of lithographic performance have been investigated as described in this section.

3.1 Print field size

The illuminated field of the ETS is described by a 28^{o} arc, 24 mm in cord length and 1.5 mm wide as shown in Figure 2a. The ETS field of view is the largest high resolution EUV field of view demonstrated to date. Operating in step-and-scan mode, the print field of the ETS is extended in the scan dimension to 32.5 mm as shown in Figure 2b. This is the first demonstration of an EUV printed field large enough for commercial IC manufacture. The printed mask pattern contains a variety of bright field and dark field features designed to characterize imaging performance at feature sizes as small as 80 nm. In the ETS initial configuration using a 40 watt drive laser, long scan times are required to print full field images. The goal of the full-power upgrade is to reduce the scan time to a few seconds.

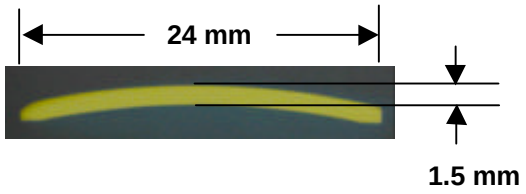

Figure 2a. ETS illuminator provides uniform illumination over a 28^{o} arc shown above.

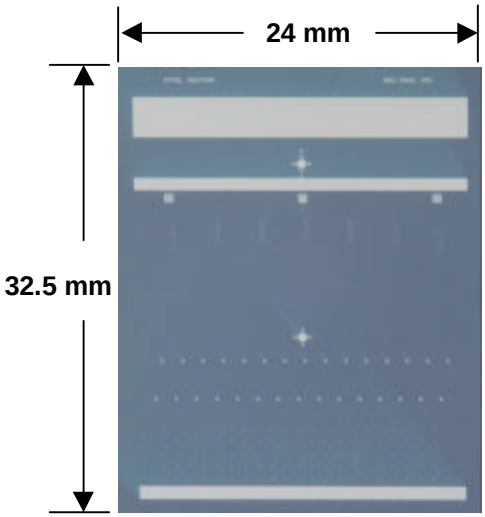

Figure 2b. The ETS print field in step-and-scan mode is extended to 32.5 mm in the scanned dimension. This print field is the largest high resolution EUV print field demonstrated to date.

3.2 Astigmatism correction

The first objective in lithographic characterization of the ETS was to find best focus at the central field point. Figure 3 shows images of 100 nm iso/dense elbow patterns acquired in a through-focus series. Analysis of these images at various focus positions reveals a small amount of astigmatism. The best focus position for horizontal lines occurs at 1 micron above the best focus position for vertical lines. Comparison of these results to simulated images, indicates that best agreement with these images is obtained when - 0.5 nm of astigmatism is added to the model. Modeling further showed that an additional 0.5 nm of astigmatism provides the optimum performance for 100 nm features. Therefore, a correction of +1 nm of astigmatism was added to the projection system by tilting the fourth imaging mirror in situ.

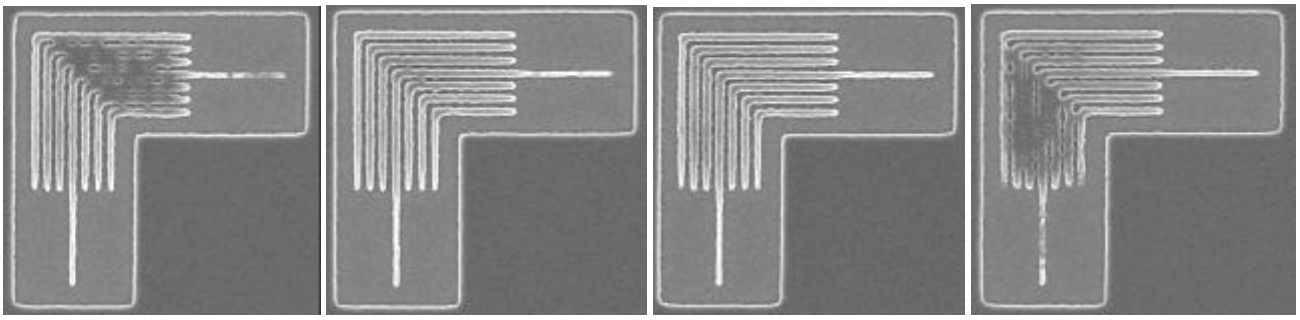

Figure 3. Through–focus images of 100 nm iso/dense elbows at the central field point prior to correction for astigmatism. The horizontal lines are out of focus in the far-left image, while the vertical lines remain in focus. The opposite condition is evident in the far-right image.

Adjustment for astigmatism is performed in a similar manner in commercial lithography tools operating in the deep ultraviolet. The resulting images, shown in Fig. 4, demonstrate that the astigmatism was corrected. Since the required adjustment was exceedingly small, the PO Box has clearly demonstrated excellent stability during the 9 months it was installed in the ETS, prior to the recording of these images. During this time the PO Box was removed and installed three times in the course of system integration activities. Stable performance of PO Box 1 has been observed for an additional 5 months, since these images were recorded.

Through-focus images were printed throughout the static field of view to identify wafer tilt deviation from the image plane of the projection system. The wafer was tilted to agree with the plane of best focus by commanding the wafer stage to rotate through the desired angles. A capacitive focus system, that senses both the vertical displacement and the out-of-plane tilts, is used as a control to reproduce across-plane focus on subsequent wafers as required to print scanned images.

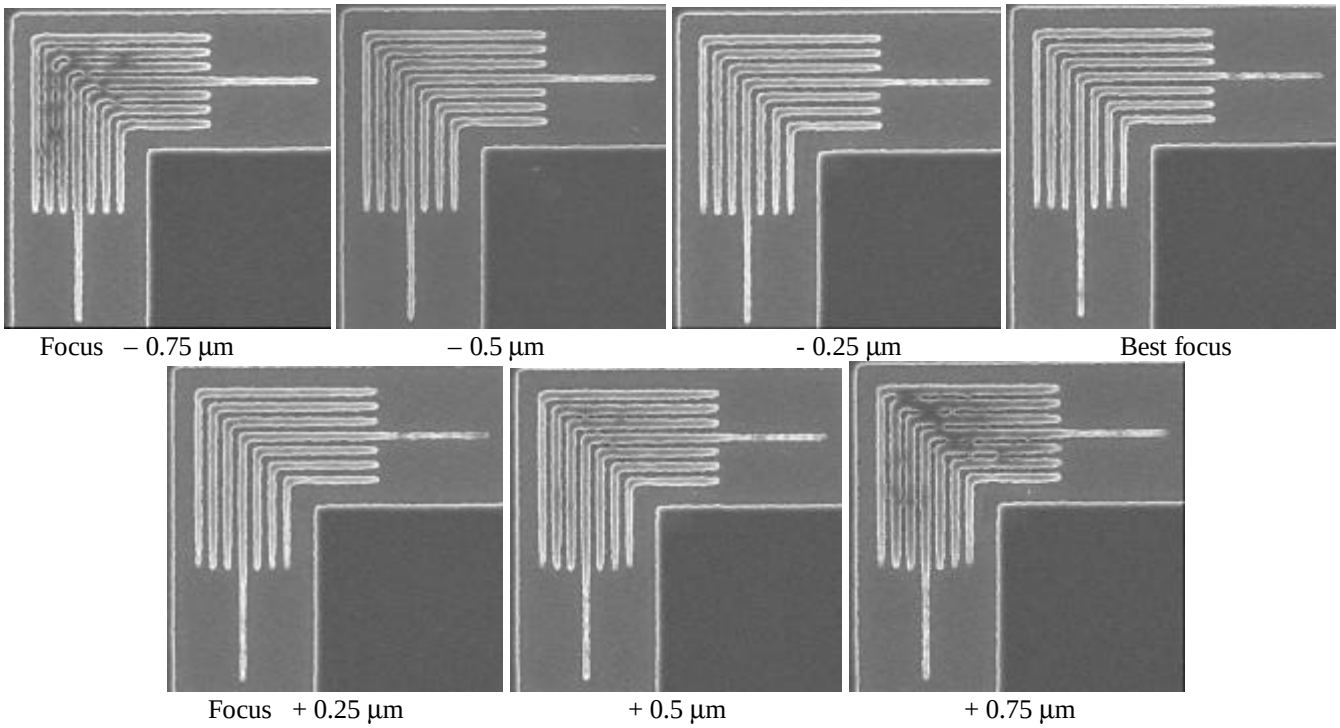

Figure 4. Through-focus images of 100 nm iso/dense elbows at the central field point after correction for astigmatism. At 0.75 µm on either side of best focus, the horizontal and vertical lines are going out of focus together, indicating that the alignment has been optimized with respect to astigmatism.

3.3 ETS pupil-fill effects

In the ETS the pupil fill consists of six channels to approximate a $s = 0.7$ pupil fill[2]. Each channel of the condenser system provides Köhler-critical illumination that gives an arc-shaped intensity profile to match the POB ring field and an angular distribution of approximately $s_V = 0.3$ and $s_H = 0.015$. That is, the fill for a single channel is essentially coherent in the horizontal direction. For a single channel, images that diffract light in the horizontal direction (ie. vertical lines) will exhibit coherence effects (here, horizontal is perpendicular to the scan direction). In the incoherent sum of images formed from all six channels these coherence effects will be diminished as desired. However, both modeling and experiment show ringing effects in images of vertical lines that can be attributed to the six-channel pupil fill. An example of this is shown in Fig. 5, where simulated aerial images of 100 nm 1:1 dense elbow patterns are compared for the ETS six-channel fill (a) and a conventional $s = 0.7$ top-hat fill (b). It is seen that faint "ghost images" of the pattern appear with the ETS fill, and the vertical lines of these ghost images are stronger than the horizontal lines. Where the vertical ghost lines intersect with the desired elbow pattern they add intensity. In a resist-printed image this causes a periodic variation in the linewidth, especially of the horizontal lines. A variation in the linewidth of as much as 20 nm is expected. This effect is observed experimentally and is more apparent in underdosed prints. A static print from the ETS is shown in Fig. 5(c), where the horizontal lines show a larger variation in linewidth than the vertical lines. Although this effect is subtle when viewed directly by eye, it is significant and must be accounted for when performing studies of line edge roughness or defect printability in the ETS. This effect will not be present in commercial EUV tools, which will employ illuminators with conventional fills.

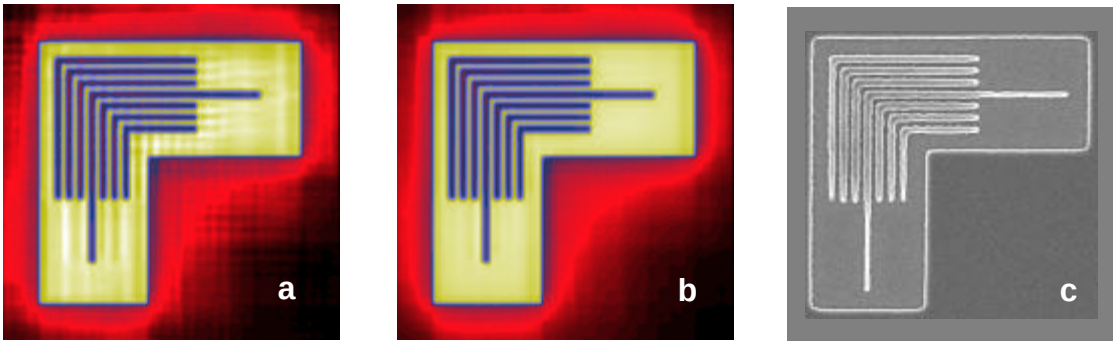

Fig 5. Simulated aerial image of 100 nm dense 1:1 elbows with the six-channel ETS pupil fill (a) and conventional top-hat fill (b). A resist print of 100 nm elbows is shown in (c).

3.4 Skew and scan magnification

To operate in step and scan mode it is necessary to match scan speed of the wafer stage to that of the scanning aerial image. Equivalently, the scan magnification (ratio of wafer-stage to reticle-stage speeds) must match the optical magnification of the projection system. If this parameter is not matched, the horizontal features, which have structure in the scan direction, will be degraded by motion blur (See Figure 6a).

A similar degradation occurs if the scan direction of the wafer stage is not matched to that of the scanning aerial image. This affect can be stated in terms of stage skew, which is the angle between the scanning axes of the wafer stage and the reticle stage. The stage skew must match the skew between the scan direction of the aerial image and that of the wafer. Skew can be introduced by the projection system or by misalignment between the wafer metrology system and the reticle metrology system. If this parameter is not matched, the vertical features, which have structure in the cross-scan direction, will be degraded by motion blur (See Figure 6b).

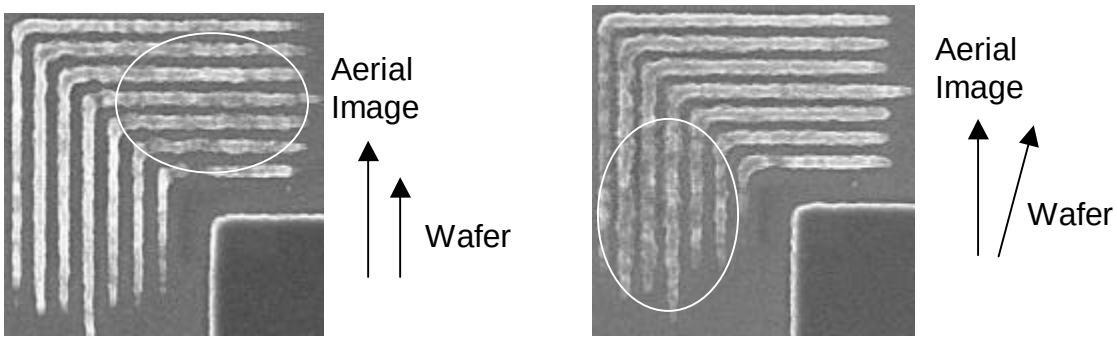

a b

Figure 6. (a) Scanned image degraded by magnification error, where the aerial image and the wafer move at different speeds. (b) Scanned image degraded by skew error, where the aerial image and the wafer move in different directions.

To determine the optical magnification cross-hair marks were printed in resist throughout the ring field. A Leika Ipro tool was used to measure the separation between the marks. These measurements were compared to the known separation of the marks on the reticle. To achieve agreement in the central field region the optical magnification was 82 ppm greater than the nominal ¼ magnification. This difference is within the expected range and easily corrected by adjusting the scan speed ratio. The magnification correction was confirmed by recording images at various scan speed ratios and observing the best results for horizontal feature to be at a magnification adjustment of +75 ppm, which is in good agreement with the Ipro measurements.

The determination of skew from printed images of Ipro marks is also possible in principle. This process is complicated by the non-telecentric reticle illumination, which couples reticle roll into the printed location of the Ipro marks. A procedure for extracting skew from a sequence of printed images was developed but not implemented to support first scanned imaging experiments. Skew was found by printing images at various skew angles and maximizing the contrast of the dense vertical lines. This process resulted in an optimum skew angle of –680 microradians in the ETS coordinate system. The scanned image, resulting from these corrections in scan magnification and skew, is shown in Figure 7

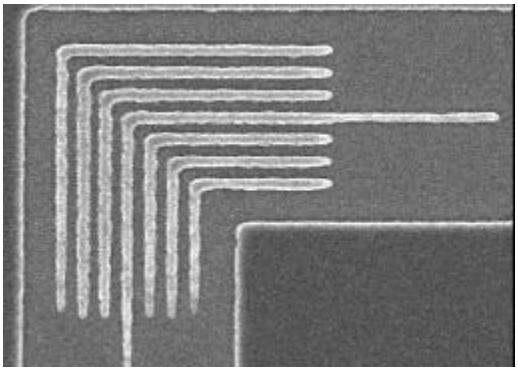

Figure 7. Scanned image of 100 nm iso/dense elbows using a magnification correction of +75 ppm and a skew correction of – 680 micro radians.

3.5 Lithographic flare measurements of the PO Box 1

Flare is caused by the light scattering from the optical components of a projection system. As the feature size of the printed circuit gets smaller, the importance of flare is also enhanced. Scattering redirects the light from an area of an image intended to be bright into all areas of the image, including those regions intended to be dark. The resulting background illumination within the image field is called flare, and it reduces image contrast and shrinks the process window. Mid-spatial frequency roughness of the imaging mirror surfaces creates the flare.

The magnitude of the flare is proportional to $1/\lambda^2$. Thus, as the wavelength in the lithographic system gets smaller, the effects of flare increases. Since EUV wavelengths are shorter than the conventional DUV wavelengths by an order of magnitude, understanding the flare contribution to the printed features is critical.

EUV flare can be directly identified by measuring the extended point spread function of the projection system, but it requires a coherent EUV source such as a synchrotron. As an alternate method, flare can be lithographically measured by printing dark features in the bright field region. Lithographic measurement of flare has been performed with the ETS. Flare for a given feature size is determined by dividing the dose to clear the bright region, E_0, by the dose to clear the dark feature, E_D.

Dark square features, in the size ranging from 1 μm to 4 μm, are located in the central area of the bright field region of the mask. This bright field was exposed onto a wafer with various dose levels at an increment of 15%, until the given dark features disappear completely. The 4 μm square feature is shown in Fig. 8 as the dose approaches E_D, and the feature washes out. The flare at the center of the smile field is determined to be ~40% based on a 4 μm square. The calculated flare values, using the actual power spectral density of the imaging mirror surfaces, and the lithographically measured flare values of the PO Box 1 for the central field point are plotted in Fig. 9. The predicted and measured values agree to within the error bar, associated with the chosen dose increments.

Figure 8. Flare features printed with a 15% dose increment per image from left to right.

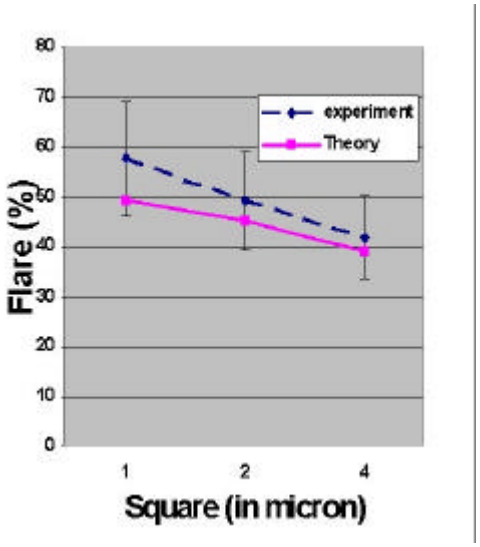

Figure 9. Flare measured lithographically compared to theory based on mirror roughness.

3.6 Aerial Image Monitor

An Aerial Image Monitor, AIM, has been installed and tested in the ETS. This sensor is designed to characterize the EUV aerial image directly by using an AIM artifact, comprised of narrow (100 nm) slits in a 200 nm nickel absorber deposited on a 100 nm silicon nitride membrane. The radiation, passing through a slit and transmitted through the membrane, is detected using an EUV-sensitive detector[3]. This arrangement is shown schematically in Fig 10.

To achieve high spatial resolution the slit width is restricted to 100 nm or smaller. In this case the measured slit width was 90 nm. While the narrow slit provides high spatial resolution, it limits the collection of light and thereby reduces the sensitivity and signal-to-noise ratio. To increase the collection area, the slit length is extended to 100 μm, and the slit is replicated 10 times on a pitch of 10 μm. This pattern can be used to characterize a one-dimensional feature on the reticle that is replicated on a 40 μm pitch to produce a 4x-reduced image that matches the pitch of the AIM artifact.

The AIM detector was tested using a reticle pattern comprised of 20 line pairs of length 200 μm and width 5 μm, when imaged at the wafer plane. To avoid loss of resolution due to misalignment of the reticle and AIM artifact, alignment in all rotational axes must be performed to 100 microradians or better. A coordinate measuring machine was used to assure that the artifact and reticle were angularly aligned to the respective stage platens, to which angular orientation is referenced by the stage metrology system. The maximum alignment error was 32 microradians. Stage rotations can be used to correct for larger rotational errors, but that was not required in this case, due to the high alignment accuracy.

In the initial test the AIM artifact was positioned near the middle of the aerial image of the reticle pattern, which is twice as large as the series of slits on the AIM artifact. The reticle and AIM features, used in the initial experiments, have the long

dimension in the scan direction. The wafer stage, carrying the AIM sensor, was then translated in the cross-scan direction in 50 nm increments, and the signal level was observed as the AIM slits travel a distance of 10 μm or one cycle of the reticle pattern. The results are shown in Fig. 11.

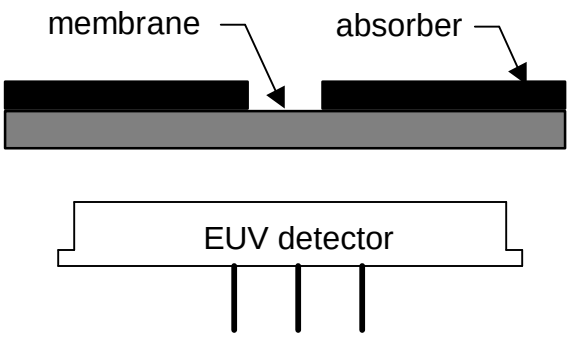

Figure 10. Sketch of Aerial Image Monitor sensor

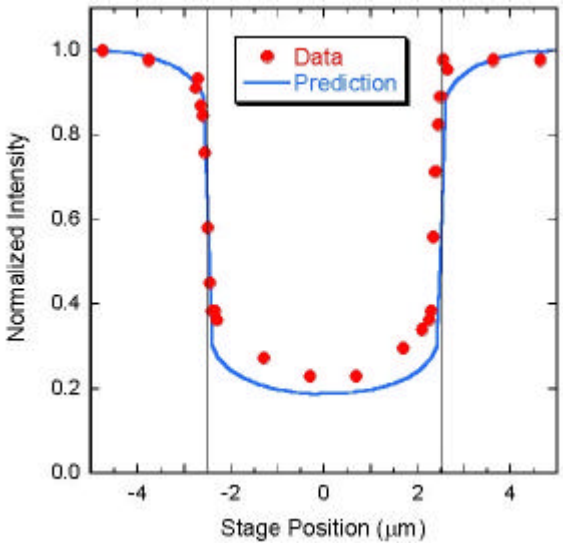

Figure 11. AIM scan compared to simulated image.

The relative intensity measured in the middle of the dark lines at stage position 0 is nonzero due to the relative high level of flare in PO Box 1. The prediction agrees with the observed magnitude of illumination. A steep slope is evident as the slit traverses the edge of the absorber at stage positions of ±2.5 μm. The transition from bright to dark, which occurs in a distance of 150 nm to 200 nm, indicates that the AIM artifact is in focus. The out-of-focus condition results in a lesser slope at the edge of the reticle features. One of the applications of AIM is to find focus in near real time without the need for resist exposures. AIM can also be used to measure drift and jitter between the aerial image and the wafer and to measure scan distortion.

4. SYSTEM UPGRADES

Two major upgrades are in progress to increase EUV throughput and increase resolution. The throughput upgrade will incorporate a 1700 watt drive laser and a xenon spray jet nozzle for increased source power in the EUV. The resolution upgrade will integrate an improved projection system, PO Box 2, having lower figure error and lower flare. Upgrades in the stage system, sensors and controls are also required to support operation at high power and high resolution.

4.1 High-power source integration

The high power laser is a three-chain pulsed Nd:YAG system developed by TRW and described previously[4]. The beam from each chain is focused to a common point on the target to drive the plasma. The target system is being upgraded to a xenon liquid spray jet depicted in Fig. 12. Liquid xenon is forced through a cooled nozzle, producing a fine spray of xenon droplets which are heated by the incident laser beam to form the EUV-emitting plasma. Recent experiments have demonstrated a conversion efficiency from laser energy to in-band EUV radiation of 0.5%. Since xenon has demonstrated conversion efficiency in excess of 0.5%[5], further improvements are expected.

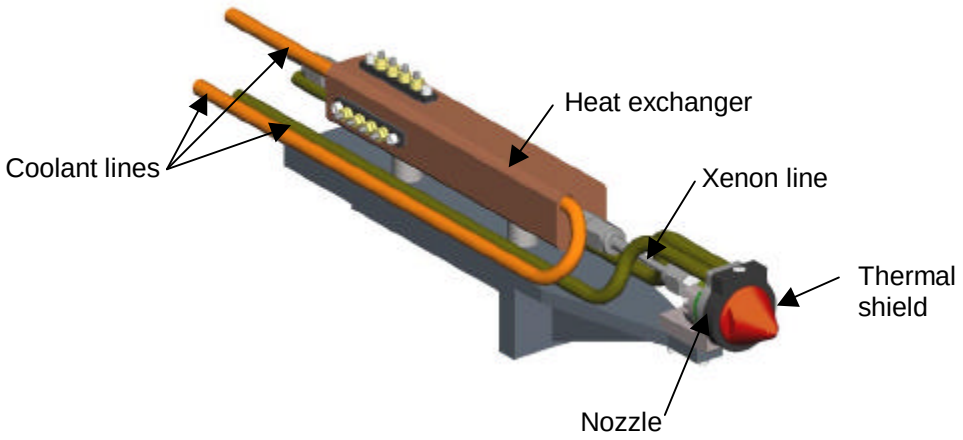

Figure 12. TRW liquid spray jet engineered for ETS compatibility.

4.2 PO Box 2 imaging

To enable the earliest possible imaging demonstration with the ETS Set-2 optic and verify the alignment interferometry, static, sub-field printing capabilities have been added directly to the at-wavelength system-level interferometer at LBNL[6]. PO Box 2 has a wavefront error of ?/24 measured at the central field point, compared to ?/14 for PO Box 1. The sub-field exposure station (SES)[7] has an illumination field size of approximately 100 μm at the wafer, however, the full 1-inch arc field can be covered one sub-field at a time. The SES uses the same reflection mask technology as used in the ETS.

The SES is installed on an undulator beamline at Lawrence Berkeley National Laboratory's Advanced Light Source synchrotron radiation facility. In order to reduce the inherent coherence of the undulator beamline optimized for high accuracy interferometry[8], an active scanning mirror illuminator has been developed. This allows the SES imaging to be performed with illumination having a lithographically relevant partial coherence (σ). The active illuminator supports variable σ ranging from approximately 0.1 to 1. The images shown in Fig. 13 were printed using a conventional tophat fill with a σ of 0.62.

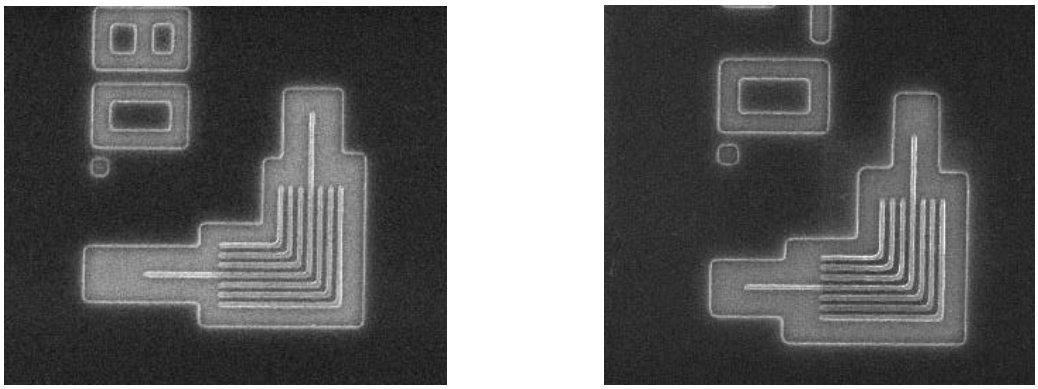

Figure 13. PO Box 2 images recorded in the sub-field exposure station showing 80 nm iso/dense elbows (left) and 70 nm iso/dense elbows (right).

The performance of PO Box 2 is clearly superior to that of PO Box 1. Although there are a number of differences between the ETS and the SES, such as the condenser and associated pupil fill factor, the improvement in image quality is greater than these differences can explain. PO Box 1 images of Fig. 4 clearly show iso-dense bias as evidenced by the isolated lines being narrower than the dense lines in the same image. In PO Box 2 images of Fig. 13 the isolated lines show very little thinning relative to the associated dense lines even at the smaller resolution of 70 nm. We can conclude that PO Box 2 performance at 70 nm feature size is better than that achieved by PO Box 1 at 100 nm.

5. SUMMARY

The ETS has demonstrated the capability to print 100 nm features in both static mode and step-and-scan mode. This result was achieved using a developmental projection system and a low power (40 watt) drive laser for the plasma source. Initial lithographic characterization found a weak astigmatic aberration in the projection system that was corrected by in situ adjustment as is commonly done in advanced optical lithographic tools. The projection system has demonstrated stable operation for a period of more than one year from the time it was aligned and first installed in the ETS. An EUV-sensitive aerial image monitor has been used to acquire initial aerial image profiles that are in good agreement with the image model. High resolution full-field images, measuring 24 mm by 32.5 mm have been printed, demonstrating the feasibility of printing die sites that meet the size requirements of commercial IC manufacture.

The ETS performance upgrades are in progress to increase EUV throughput and image resolution. The goal of full-power source integration is to reduce exposure times and achieve a scan speed of 10 mm/s. Using the improved projection system, which has printed 70 nm features in sub-field images, the resolution goal is to achieved 70 nm resolution in full-field scanned images.

ACKNOWLEDGMENTS

The authors are indebted to the members of the subsystem teams and technology teams, whose hard work is responsible for advancing the EUV Engineering Test Stand to the state of development reported in this paper.

This work was performed by the University of California Lawrence Livermore National Laboratory under the auspices of the U.S. Department of Energy, Contract No. W-7405-ENG-48, by Sandia National Laboratories under the auspices of the U.S. Department of Energy, Contract No. DE-AC04-94AL85000, and by the Lawrence Berkeley National Laboratory under the auspices of the U.S. Department of Energy Office of Basic Energy Sciences. Funding was provided by the Extreme Ultraviolet Limited Liability Company under a Cooperative Research and Development Agreement.

REFERENCES

1. D. A. Tichenor, A. K. Ray-Chaudhuri, W. C. Replogle, R. H. Stulen, G. D. Kubiak, P. D. Rockett , L. E. Klebanoff, K. L. Jefferson, A. H. Leung, J. B. Wronosky, L. C. Hale, H. N. Chapman, J. S. Taylor, J. A. Folta, C. Montcalm, R. Soufli, E. Spiller, K. Blaedel, G. E. Sommargren, D. W. Sweeney, P. Naulleau, K. A. Goldberg, E. M. Gullikson, J. Bokor, P. J. Batson, D. T. Attwood, K. H. Jackson, S. D. Hector, C. W. Gwyn, and P. Y. Yan, "System Integration and Performance of the EUV Engineering Test Stand," *Emerging Lithographic Technologies V*, Proceeding of SPIE, **4343**, pp. 19-37, 2001.
2. H. N. Chapman, A. K. Ray-Chaudhuri, D. A. Tichenor, W. C. Replogle, R. H. Stulen, G. D. Kubiak, P. D. Rockett , L. E. Klebanoff, D. O'Connell, A. H. Leung, K. L. Jefferson, J. B. Wronosky, J. S. Taylor, L. C. Hale, K. Blaedel, E. Spiller, G. E. Sommargren, J. A. Folta, D. W. Sweeney, E. M. Gullikson, P. Naulleau, K. A. Goldberg, J. Bokor, D. T. Attwood, U. Mickan, R. Hanzen, E. Panning, P.-Y. Yan, C. W. Gwyn, and S. H. Lee, "First Lithographic Results from the EUV Engineering Test Stand," submitted to *J. Vac. Sci*. 2001.
3. K. W. Berger and R. H. Campiotti, "Absolute Dosimetry for Extreme Ultraviolet Lithography," *Metrology, Inspection, and Process Control for Microlithography XIV*, Proceedings of SPIE, **3998**, pp. 838-845, 2000.
4. G. D. Kubiak, L. J. Bernardez, K. Krenz, W. C. Replogle, W. C. Sweatt, D. W. Sweeney, R. M. Hudyma, and H. Shields, "High-power source and illumination system for extreme ultraviolet lithography," Proceedings of the SPIE **3767**, p. 136, 1999.
5. P. D. Rockett, J. A. Hunter, G. D. Kubiak, K. Krenz, H. Shields, and M. Powers, "Detailed EUV Characterization of Laser-Plasma Sources for EUV Lithography," OSA Proceedings on Extreme Ultraviolet Lithography, F. Zernike and D. T. Attwood, eds. **23**, pp. 255-259, 1994.
6. P. Naulleau, K. Goldberg, E. Anderson, P. Batson, P. Denham, S. Rekawa, and J, Bokor, "At wavelength characterization of the Engineering Test Stand Set-2 optic," submitted to *J. Vac. Sci. & Technol. B*, 2001.
7. P. Naulleau, K. Goldberg, E. Anderson, P. Batson, P. Denham, S. Rekawa, and J. Bokor, "Adding static printing capabilities to the EUV phase-shifting point diffraction interferometer," *Emerging Lithographic Technologies V*, Proceeding of SPIE, **4343**, pp. 639-645, 2001.
8. D. Attwood, P. Naulleau, K. Goldberg, E. Tejnil, C. Chang, R. Beguiristain, P. Batson, J. Bokor, E. Gullikson, H. Medecki, and J. Underwood, "Tunable coherent radiation in the soft X-ray and extreme ultraviolet spectral regions," *IEEE J. Quantum Electron.* **35**, pp. 709-720, 1999.